Flinders UNIVERSITY

Implementation of Antireflection Layers for Improved Efficiency of Carbon Nanotube-silicon Heterojunction Solar Cells

LePing Yu [a], Daniel D. Tune [a], Cameron J. Shearer [a] and Joseph G. Shapter [a1]

[a] Centre for Nanoscale Science and Technology, Flinders University, Bedford Park, South Australia 5042

Abstract

We explore the use of antireflection polymer layers on n-type silicon solar cells that use a carbon nanotube (CNT) front electrode. Three different types of polymer were studied; polydimethylsiloxane (PDMS), poly(methyl methacrylate) (PMMA) and polystyrene (PS).The influence of polymer type and thickness on device performance has been assessed. The performance degradation with ageing of Si-CNT, Si-CNT-PDMS, Si-CNT-PMMA and Si-CNT-PS solar cells has been compared. Based on the analysis of the results, antireflection polymer layers are able to reduce the reflectance of the cell surface and subsequently improve the amount of solar energy absorbed by the silicon without any detrimental effect on the photovoltaic junction. With the addition of a 75 nm PS antireflection layer, devices achieved a photovoltaic conversion efficiency of up to 7.8 % under standard AM 1.5G conditions.

Key words

Carbon nanotube; Polymer antireflection film; solar cell; renewable energy

[1] Corresponding author. Centre for Nanoscale Science and Technology, Flinders University, Bedford Park, South Australia 5042.

Tel: +61 8 8201 2005. Email: Joe.Shapter@flinders.edu.au (Joseph Shapter)

1. Introduction

Some ten years ago Richard Smalley defined the most pressing issues facing humanity [1]. These included the production of cheap, reliable energy, provision of clean drinking water and the effective treatment of major disease. While is little doubt that these are still the major issues, it is clear that energy is the single most pressing issue facing humanity in the 21st century. As society becomes more technologically advanced and a greater proportion of the Earth's population has access to that range of technology, energy requirements will reach unprecedented levels. The current forms of energy production clearly can't be used to satisfy these requirements as the environmental damage would be unacceptable and the finite resources would be depleted very quickly. Solar power represents the obvious solution to provide these energy requirements but ways to harvest it cheaply and with the minimal environmental footprint must be found. These increasing energy demands and environmental concerns regarding the use of non-renewable and polluting energy sources such as the combustion of fossil fuels have led to the need to employ alternate renewable, green and economically viable solutions. The application of solar cells to convert sunlight directly into electricity is one such method [2, 3].

Using carbon materials, the problems of high production costs, scarcity and/or toxicity of some of the materials currently used in solar cells could be solved and a stand-out example is carbon nanotubes (CNT). Carbon nanotubes are one of the allotropes of carbon and due to their excellent electrical and optical properties [4, 5], they have been applied in new generation solar cells [6, 7], such as those using CNT-Si heterojunctions [8]. The structure of a CNT-Si heterojunction solar cell is similar to that of an n-type monocrystalline silicon solar cell but with replacement of the p-type emitter layer and front contact metallization by a CNT film, which serves both purposes. Since the CNT layer is thin, photons can reach the underlying n-type silicon and be absorbed to produce electron-hole pairs (exciton) which then diffuse into a depletion region created at the CNT-Si interface. Under the influence of a built-in potential created from band-bending due to equilibration of the Fermi levels at the junction, these excitons are separated into free holes and electrons which can be collected at the CNT layer and silicon substrates, respectively [9].

The first such CNT-Si solar cell reported, with a photovoltaic conversion efficiency (PCE) of 1.3 %, used a double-walled carbon nanotube film which was deposited on an n-type silicon substrate by solvent-based casting[10]. Later, post-treatments of the device, such as with

thionyl chloride ($SOCl_2$) or acids, were developed to improve PCE [11, 12]. Similar devices were also reported using the CNT deposition method of Wu [4] which involves vacuum filtration of CNT onto mixed cellulose ester (MCE) membranes which can then be removed by dissolution with acetone [13]. Application of a gate potential to alter electronic junction properties (via ionic liquid electrolyte) was reported to adjust efficiency between 4 and 11 % reversibly and dynamically, and this was interpreted to be due to the modulation of carbon nanotube Fermi level and improvement of the homogeneity of the silicon depletion region [14]. Even higher PCE solar cells (13.8 %) have been reported in which nanotubes were doped *in situ* by nitric acid (HNO_3), where a decrease of tube-tube resistance and shifting of Fermi level down into the valence band contributed to high efficiency [9]. In another work, an insulating polymer poly(dimethylsiloxane) (PDMS) layer, which acted as both an antireflection (AR) and surface protection layer, was deposited onto the active area and the resultant encapsulated device showed improved PCE (> 10 %) and stability (relatively stable with 20 days in air) [15]. Recently, work focusing on using another polymer layer, poly(methyl methacrylate) (PMMA) acting as a broad band antireflection layer over Si-CNT solar cells was conducted and PCE was improved from 7.1 % to 11.5 % by increasing light trapping efficiency [16]. Some of the best Si-CNT solar cells to date have a PCE of 15 %, using a titanium dioxide antireflection layer and doping of the CNT film with oxidative chemicals (HNO_3 and H_2O_2) [17]. More recent work has reported has reported efficiencies of 17 % [18]. It is worth noting that this was achieved with a much smaller active area than is common in the field and as such, the work by Shi is likely a better efficiency benchmark.[17]

Here, we systematically explore polymer antireflection layer-related approaches that can improve the performance of Si-CNT devices, structured as shown in Figure 1. Specifically, three kinds of polymers including PDMS, PMMA and poly(styrene) (PS) have been implemented as top antireflection layers to improve the amount of solar energy that reaches the silicon surface. Additionally, PS layers with different thicknesses have been added on top of Si-CNT devices to study the influence of polymer layer thickness and the performance degradation rates with ageing of Si-CNT, Si-CNT-PDMS, Si-CNT-PMMA and Si-CNT-PS cells have all been compared.

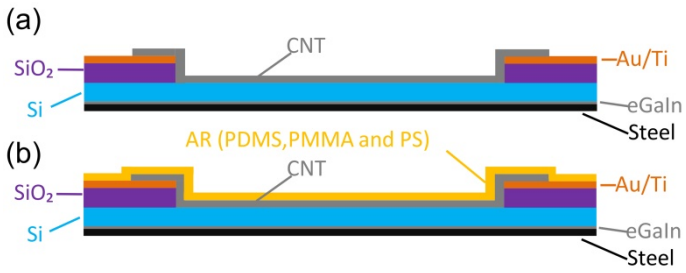

Figure 1: Schematic structures of (a) Si-CNT and (b) Si-CNT-AR. Au/Ti is used for the front contact electrodes with the back ohmic contacts made by eGaIn, which is also used to mount the cells onto steel backing plates.

2. Material and Methods

2.1 Preparation of CNT suspension

Commercial high purity CNT powder (5 mg, P3-SWNT, Carbon Solutions Inc, USA), produced by arc-discharge, was bath sonicated in aqueous TritonX-100 (50 mL, 1 % v/v, Sigma-Aldrich, Australia) for 1 h at room temperature. The suspension was centrifuged at 17 500 g for 1 h, and then the supernatant was collected and centrifuged for a further 1 h at 17 500 g. The second supernatant was then used in the following section.

2.2 Preparation of stock solution of polymers

AR polymers were deposited from solutions. A mixture of PDMS prepolymer and curing agent (10:1; weight ratio, Sylgard 184, Dow Corning, Midland, MI) was stirred and mixed completely and degassed under vacuum. The PMMA solution was prepared by dissolving solid PMMA (M_w: 120 000, Sigma-Aldrich, Australia) in acetone with the concentration of 2.2 wt%. PS solutions were prepared by dissolving PS (M_w: 230 000, Sigma-Aldrich, Australia) in toluene with the concentration of 1.85 wt%, 2.2 wt% and 2.85 wt%.

2.3 Assembly of solar cells

460 µL cm^{-2} of CNT suspension was diluted in 250 mL aqueous TritonX-100 (0.01 % v/v) to achieve CNT films with 70 % transmittance. The diluted CNT suspension was then filtered onto a target mixed cellulose ester (MCE) membrane (0.45 µm, HAWP, Millipore, Australia) with the assistance of a nitrocellulose ‘stencil’ membrane with 4 × 0.49 cm^2 holes (25 nm, VSWP, Millipore, Australia). The difference between pore sizes of the two membranes enables fast flow rate at through the four cut-out areas and four identical CNT membranes could be collected in one filtering. Then, CNT films were rinsed with 3 X 50 mL water followed by a further 250 mL of water in order to remove any remaining surfactant. For

device fabrication, a central circular area (0.32 cm^2) was cut out from each membrane. Phosphorous doped n-type silicon wafers (5-10 Ω cm, 525 μm thick with a 100 nm thermal oxide, ABC GmbH, Germany) were used as substrates for the devices. Positive photoresist (AZ1518, micro resist technology GmbH, Munich, Germany) was applied by spin coater (3000 rpm, 30 s) on the Si and soft-baked at 100 °C for 60 s. A mask was put on this resist and UV photolithography defined an active area (0.079 cm^2), which was developed by developer (AZ 326 MIF, AZ electronic Materials, GmbH, Munich, Germany) and Ti/Au (5/145 nm/nm) was sputtered (with deposition controlled by quartz crystal microbalance, Quorumtech K757X) as the front metal contact. Then, the photoresist was lifted off by immersion in acetone for 30 min. One drop of buffer oxide etch (BOE, 6:1 of 40% NH_4F and 49% hydrofluoric acid (HF), Sigma-Aldrich, Australia) was used to etch the front 100 nm thermal oxide layer. The circular CNT/MCE films were placed on top of the substrates (CNT side down). A drop of water was used to wet the film and the device was then baked at 80 °C for 15 min. After cooling, the substrate with CNT/MCE was immersed in 3 sequential baths of clean acetone (30 min each) to dissolve the MCE. Following scratching of the back oxide layer of silicon, a gallium indium eutectic (eGaIn) was used to mount cells onto stainless steel plates (Figure 1). The resulting cells are ‘as prepared’ devices. To determine transmittance and sheet resistance, CNT/MCE films were applied onto a glass slide and the same procedure was conducted to dissolve MCE. Antireflection layers were applied onto cells after all post treatments described in the next section. PDMS films were simply transferred to cells while PMMA and PS films were spin-coated at 6500 rpm for 90 s.

2.4 Post treatments to devices

The as-prepared devices were subjected to three post treatments. First of all, an HF (2 %) treatment was used to etch the oxide layer which was formed during the cell fabrication process on top of silicon surface in the active area. This was achieved by putting 1 drop on top of the device for 10 s followed by rinsing with water and ethanol. Since HF can dissolve glass, it was replaced by HCl in the same manner to measure the transmittance and sheet resistance of the films on glass. $SOCl_2$ treatment was conducted by placing 2 drops onto the surface of the cells/glass slides and then the surface was allowed to dry, rinsed with ethanol and then blown dry with N_2. This is used to improve the conductivity of the film by electron transfer from the CNT to organic oxidizer [12]. The second HF treatment was conducted in the same manner as the first in order to etch the oxide layer induced by the $SOCl_2$ treatment and this allowed observation of the effect of the $SOCl_2$ treatment.

2.5 Characterization and measurements

Transmittance of CNT films was calculated from absorbance spectrum measured by UV-Vis-NIR spectrophotometry. Light passed through CNT films mounted on a glass slide and a clean glass slide acted as background sample. The transmittance value is averaged from 2 wavelengths (450 and 850 nm). Reflectance spectra were measured by a Perkin Elmer UV-Vis-NIR Lambda 950 spectrometer from 350 to 1500 nm. CNT films (d=1.8 cm) were attached onto a silicon wafer (2.5 X 2.5 cm) and different polymer layers were coated on it (PDMS: simple transfer; PS & PMMA: spin coating). Data in the range of 850 to 1050 nm was excluded due to the significant error caused by the change of the light source in the instrument. Conductivity/sheet resistance of the CNT film which was attached onto a glass slide was measured by a four point probe (Keithlink). Polymer thicknesses were determined by Atomic Force Microscope (Nanoscope, Multimode, Bruker) by applying films onto silicon surfaces. In order to detect the thickness of the surface, a few scratches were made by a surgical scalpel. A Keithley 2400 source measure unit was used to collect current-voltage data which were recorded by using a custom Labview^{TM} virtual instrument for all devices. The power density at the sample plane of the collimated xenon-arc light source, which was passed through an AM 1.5G filter, was 100 mW cm^{-2} as determined by a standard silicon test cell with NIST-traceable certification.

3. Results and discussion

3.1 The as prepared devices and the effect of the post treatments

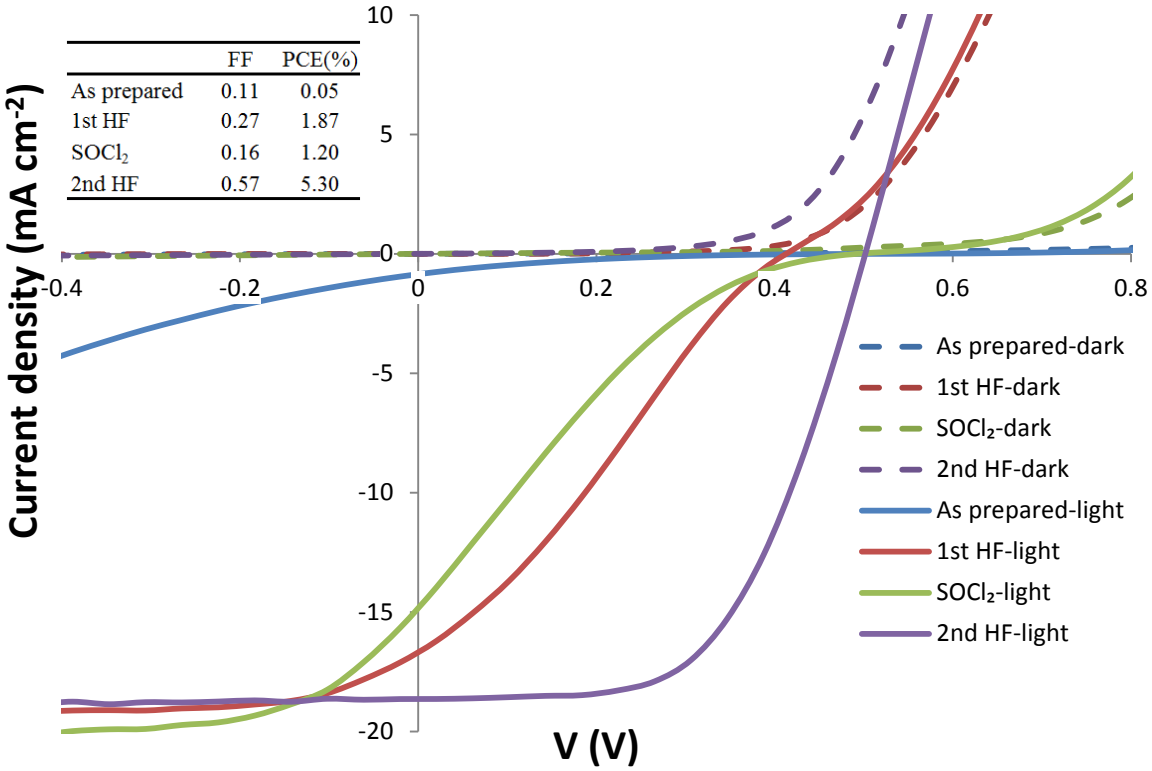

Figure 2: Representative current density-voltage (J-V) curves (solid lines: light curves; dashed lines: dark curves) of Si-CNT cells before and after different treatments (the first HF, $SOCl_2$ and the second HF); the inset table shows the change of fill factor (FF) and photovoltaic conversion efficiency (PCE) for these curves.

Figure 2 shows the influence of different treatments on the performance of Si-CNT cells (both dark and light curves). As prepared devices always have low PCE due to limited short circuit current density (J_{sc}) and poor fill factor (FF). This is caused by the growth of relatively thick oxide layer on the silicon surface during thermal and wet fabrication processes. This thick oxide layer can block charge carrier transfer through the interface. After the first HF treatment, the SiO_x layer is removed and PCE increases to about 2 %. The purpose of $SOCl_2$ treatment is to increase the conductivity of the CNT membrane via p-type doping effect by extracting electrons from the top of the valence band of the CNT. The resulting devices usually have poorer performances than the one after the first HF because $SOCl_2$ is able to react with silicon surface and create a thin SiO_x layer again. After the second HF treatment, the FF and PCE improve from 0.27 to 0.57 and 1.87 % to 5.3 %, respectively, for this particular cell. By analyzing the dark curves using the thermionic emission model [19], diode properties of the device have improved after the 3 treatments, with both ideality and reverse

saturation current density (J_{sat}) reduced, as shown in Table S1.

The ultraviolet-visible-near-infrared spectra of a CNT film before and after different treatments are shown in Figure 3 (a). In the as-prepared sample, the S_{11} peak at 1850 nm indicates that there are some large-diameter carbon nanotubes and the transition energy is about 0.7 eV. The absorption peaks are broad, which indicates the expected bundled state of the dispersion as well as polychirality of CNT in the film [20]. The S_{11} peak is slightly suppressed after the first HCl treatment, which indicates that mild acid has a slight p-doping effect on CNT by protonation. As a result, the sheet resistance of the CNT film decreases slightly, as shown in Figure 3 (b). The S_{11} transition is bleached completely by $SOCl_2$ treatment because electrons are transferred from the top of valence band of CNT to the organic oxidizer [21]. This leads to a decrease in sheet resistance from approximately 700 to 350 Ω sq^{-1}. The S_{11} peak does not return after the second HCl treatment and there is no obvious change in sheet resistance indicating the second treatment does not significantly affect the population of electronic states of the CNT film.

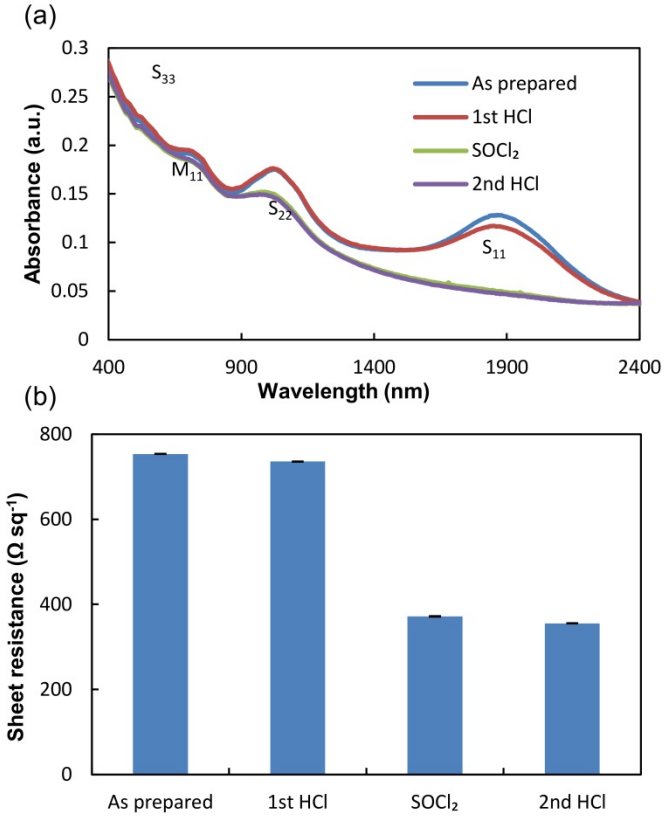

Figure 3: (a) UV-vis-NIR absorption spectra and (b) sheet resistance of large arc-discharge CNT films on glass after each treatment. Optically electronic transitions (S_{ii} and M_{ii}) of semiconducting and metallic CNT give rise to the peaks in the absorption spectra.

3.2 The effect of antireflection polymer layer on performance of the devices

As shown in Figure 4 (a), the reflectance of silicon surface with a CNT film is very high (about 30 % over a wide wavelength range from about 550 to 1050 nm where silicon can absorb energy from the incident light). Since the transmittance of all 3 types of polymers is very close to 100 % over the wavelength where silicon can efficiently produce excitons, the decreased reflectance is due to the antireflection function of polymer layers [16, 17, 22]. The PDMS film had the worst antireflection effect of all three polymers. The PMMA coated surface had its lowest reflectance near 800 nm. The particular PS layer in Figure 4 (a) exhibited a comparatively low reflectance over the whole active range of silicon. Figure 4 (b) shows the impact of antireflection polymer layers on the performance of Si-CNT devices. Clearly, adding an antireflection layer improved the performance but the three polymers showed different levels of effectiveness. The absolute increases of the PCE by adding PDMS, PMMA and PS were 0.24 % (6.17 – 5.93 %), 0.56 % (6.54 – 5.98 %) and 0.79 % (7.10 – 6.31%), respectively, as shown in Table 1. The difference of improvement is related to the antireflection effect of different polymers whereby a lower reflectance means a greater improvement in cell efficiency. In Figure 4 (a), the PS coated surface has the least reflectance and the PDMS coated surface has the highest reflectance, which is consistent with the changes in PCE after coating.

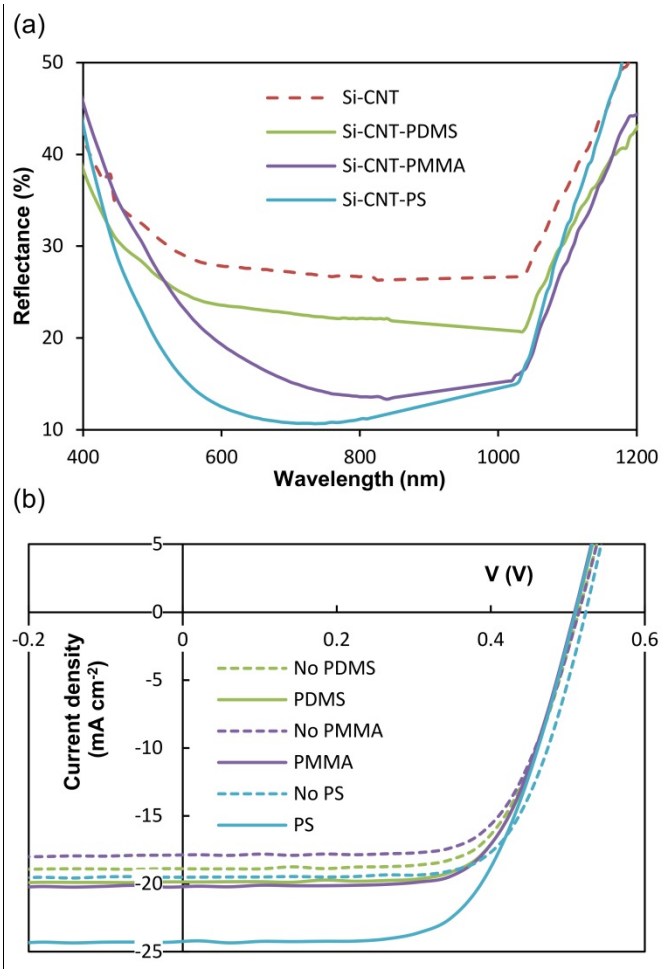

Figure 4: (a) Reflectance spectra of Si-CNT surfaces with various polymers (PDMS, PMMA and PS); the three films have different thicknesses. (b) Representative J-V curves of Si-CNT devices before and after adding various antireflection coatings (PDMS, PMMA and PS) with different thickness. Solid/dashed curves represent devices after the second HF treatment with/without antireflection polymer layers.

Table 1: Influence of different antireflection layers on the performance of Si-CNT devices. Average values with errors shown. Full error analysis is shown in Table S2 in the supplemental material. Resistances were calculated from light curves.

	No PDMS	PDMS	No PMMA	PMMA	No PS	PS
J_{sc} (mA cm^{-2})	18.4 ± 0.50	19.5 ± 0.61	17.9 ± 0.6	20.4 ± 0.72	18.4 ± 1.04	22.6 ± 1.29
V_{oc} (V)	0.50 ± 0.02	0.50 ± 0.02	0.50 ± 0.01	0.50 ± 0.01	0.52 ± 0.01	0.50 ± 0.01
FF	0.64 ± 0.04	0.64 ± 0.04	0.66 ± 0.02	0.64 ± 0.03	0.66 ± 0.03	0.62 ± 0.02
PCE (%)	5.93 ± 0.61	6.17 ± 0.66	5.98 ± 0.35	6.54 ± 0.42	6.31 ± 0.65	7.10 ± 0.68
R_{shunt} (Ohm)	4.89 ± 2.14 ×10^4	9.37 ± 0.55 ×10^4	4.48 ± 4.68 ×10^4	8.65 ± 1.02 ×10^3	7.51 ± 5.81 ×10^4	3.61 ± 5.33 ×10^3
R_{series} (Ohm)	78.6 ± 11.1	77.2 ± 13.7	76.9 ± 10.4	70.1 ± 9.78	71.7 ± 6.46	64.1 ± 4.37

R_{shunt}: shunt resistance; R_{series}: series resistance.

Table 1 provides the details of the antireflection effect of the different polymer layers on the performance of Si-CNT cells. In all cases, the J_{sc} has been improved because the silicon can

absorb more energy and more charge carriers are created and collected. Open circuit voltage (V_{oc}) remains constant for PDMS devices while there is a slight decrease of V_{oc} in both PMMA and PS devices. This might be caused by the different methods used to apply the polymer layers. During spin coating of PS or PMMA and subsequent solvent evaporation, the shrinkage of the polymer layer might apply a force to CNT films. The resulting radial strain of CNT films leads to a larger contact area of CNT with silicon while simple addition of a piece of PDMS does not change the heterojunction state [17]. This also might be the reason for slight change in FF of devices with spin-coated films.

3.3 The influence of the polymer layer thickness on the performance of the devices

Since the PS films showed the greatest improvement in PCE, further studies on antireflection optimization focused on altering the PS film thickness. By varying PS concentration (1.85 wt%, 2.2 wt% and 2.85 wt%) prior to spin-coating, thicknesses of approximately 55, 75 and 100 nm were prepared, as determined by AFM (Figure S1). As shown in Figure 5, the reflectance of Si-CNT-PS varies with PS thickness. As the thickness of PS films decreases, the wavelength (λ_{min}) at which the surface has the minimum reflectance shifts to lower wavelengths. This is consistent with double layer antireflection coating theory [23]. The minimum reflectance occurs at a wavelength where the thicknesses of both layers, polymer and CNT, are $\lambda/(8\eta_{AR})$ (η_{AR}: refractive index of antireflection layer). In this case, the thickness of the CNT film is fixed. Thus, λ_{min} decreases as the thickness of the film decreases ($\lambda_{min} = 8\eta_{AR}$ d; d: thickness of film) [23]. For silicon solar cells, absorption near 550 nm is critical for high efficiency cells and hence the position of λ_{min} is as important as the reflectance over the whole wavelength range.

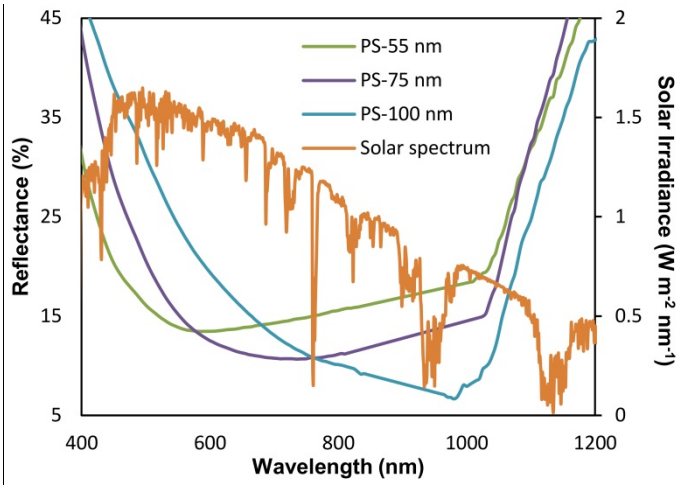

Figure 5: Reflectance spectra of Si-CNT-PS 55 nm, Si-CNT-PS 75 nm, and Si-CNT-PS 100 nm overlaid with the spectrum of terrestrial solar irradiance.

Here, the amount of light absorbed by silicon surface as a function of wavelength can defined as shown in equation 1.

$$f(\lambda) = \text{Irradiance}(\lambda)\,(1 - R(\lambda))\,T_{CNT}(\lambda) \quad (1)$$

Where Irradiance (λ) is the incident light intensity; R (λ) is the surface reflectance; T_{CNT} (λ) is the transmittance of CNT films.

Thus, the increase in the amount of light absorbed by the silicon (Δf (λ)) after adding PS films is defined by equation 2 (where it is assumed that PS films have 100 % transmittance).

$$\int \Delta f(\lambda)\, d\lambda = \int (f(\lambda)_{\text{Si-CNT-PS}} - f(\lambda)_{\text{Si-CNT}})\, d\lambda$$

$$= \int \text{Irradiance}(\lambda)\,(R(\lambda)_{\text{Si-CNT}} - R(\lambda)_{\text{Si-CNT-PS}})\,T_{CNT}\, d\lambda \quad (2)$$

where $f(\lambda)_{\text{Si-CNT-PS}}$ is the incident light absorbed by the Si-CNT-PS surface and $f(\lambda)_{\text{Si-CNT}}$ is the incident light absorbed by the Si-CNT surface. The integration is conducted from 440 to 1150 nm.

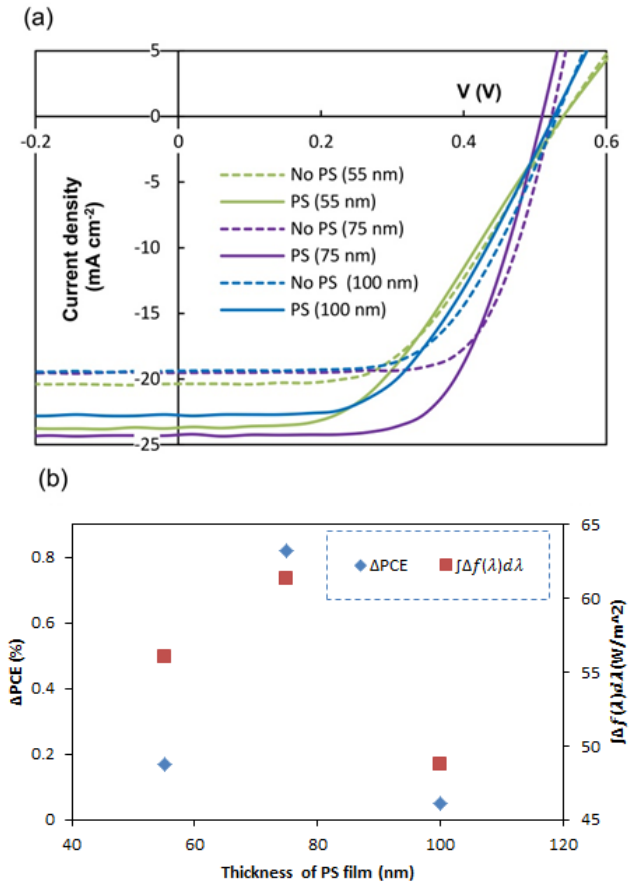

Figure 6: (a) Representative J-V curves of Si-CNT devices before and after adding PS antireflection coatings with different thicknesses where solid/dashed lines represent devices after the second HF treatment with/without PS layers and, (b) comparison of the absolute change in PCE and the absolute change in the amount of light absorbed by the surface after coating with PS layers of different thicknesses on Si-CNT devices

The absolute changes in the amount of light absorbed ($\int \Delta f(\lambda)\, d\lambda$) by surfaces coated with PS of different thicknesses (55, 75 and 100 nm) are 56.7, 61.7 and 48.7 W m^{-2}, respectively. The main improvement by adding an antireflection layer is the increased J_{sc}, which indicates more charge carriers are produced and collected [24]. As a result, the performances of devices are significantly improved, as shown in Figure 6. As the thickness of PS film changes, both ΔPCE and $\int \Delta f(\lambda)\, d\lambda$ change with a similar trend. The improvement of the PCE of the device coated with PS-2.2 wt% (75 nm) is the highest while the PCE improvement of PS-2.85 wt% (100 nm) device is very slight. There must exist an optimal PS thickness and Si-CNT device coated with that optimimal antireflection film leads to the greatest $\int \Delta f(\lambda)\, d\lambda$ and hence the best improvement on PCE. Since the thickness of the PS films has a significant influence on the shape of reflectance spectrum and the position of λ_{min}, both of which determine the value of $\int \Delta f(\lambda)\, d\lambda$, analysis about of the overall reflectance of the surface is very important in

determination of the optimal antireflection layer thickness.

3.4 Performance degradation of the devices with different structures

After confirming that AR layers were capable of significant enhancement of PCE we investigated the benefits of AR layers toward solar cell stability. The main symptom of the degradation of Si-CNT devices is the reduced FF which is related to the maintenance of the capability to separate excitons, and the likely cause of this is the growth of a silicon oxide layer. However, a top polymer layer is able to prevent oxygen from reacting with silicon surfaces to some extent. As shown in Figure 7, the decay rate of PCE from the fastest to slowest can be summarized roughly as follows: Bare > PDMS device > PS device > PMMA device. This is the expected trend due to the different O_2 permeation coefficients for the various polymers (0.23 Barrer for PMMA vs. 6. 63 Barrer for PS versus 800 Barrer for PDMS).[25-27] However, it should be noted that the thickness of the various polymer layers is not identical and this will certainly play a role as well. Additionally, the PDMS layer only has a very slight protection effect compared to the other 2 types of top polymer layers because it is not spin-coated onto silicon and this leads to a poorer sealing of surface. Interestingly, there is a slight PCE increase of the PMMA device after 1 day. This might be caused by the formation of a very thin SiO_2 layer (< 1nm) on the surface which forms a better metal-insulator-semiconductor heterojunction leading to a reduced J_{sat} [28]. The PMMA layer may provide better protection than PS because it is slightly thicker (about 130 nm compared to <100 nm). Other degradation details are shown in supplementary information Figure S2.

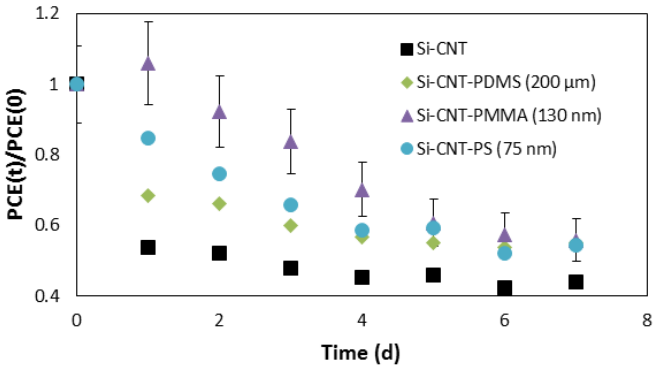

Figure 7: Degradation of Si-CNT-AR layer (PDMS, PMMA &PS) devices over 1 week; PCE (t) represents the efficiency after t days and PCE (t)/PCE (0) is the fraction to compare PCE (t) with original efficiency-PCE(0). Error bars shown are one standard deviation. The error bars for the other data are very similar but not shown for clarity.

There is an argument that adding CNT into silicon solar cells which already have efficiencies of about 25 % is unhelpful. However, the study of Si-CNT devices is still in its infancy compared to the decades of silicon solar cell development and the efficiency improvement from about 1 % in 2007[10] to 17 % in 2014 [18] has been achieved by a limited number of researchers. One significant advantage of using CNT films as a 'transparent' front electrode is the potential for reduced optical shading of the silicon base compared to some front side metallization. There are several challenges of using CNT films including how to increase the size beyond proof-of-principle laboratory scale devices and how to improve the mechanical properties. Since modification by utilizing polymers to improve the efficiency is still a new area of investigation, the amount of related literature is limited. In terms of future work, more types of polymers could be applied in this system, with device performance optimized by varying the thickness of each layer. Compared to other approaches used to improve the performance of carbon nanotube-silicon devices, such as the use of ionic liquid mediated gate potentials, polymer related modifications are easier and have a greater chance to be applied in manufacturing due to their simplicity and potentially lower costs. The price of some of the antireflection polymers used in this work (PMMA and PS) is already very low due to their industrial use. Whilst the degradation rate of thionyl chloride treated carbon nanotube-silicon devices even after adding a polymer protection layer is still quite fast, the stable efficiencies of 3-4 % obtained are still very encouraging and other regimes of p-type doping of the nanotubes show much greater stability even without polymer protection.[29] Adding more advanced multiple layer antireflection polymer systems onto the top of carbon nanotube-silicon devices will not only improve performance but increasing polymer thickness will also help to achieve better isolation of the junction from atmosphere. There are still many challenges to be solved before large scale fabrication becomes viable, including the cost of the materials and the development of proper scale-up manufacturing processes, but the potential of these systems is very exciting.

4. Conclusion

By preparing and comparing four types of device (Si-CNT, Si-CNT-PDMS, Si-CNT-PMMA and Si-CNT-PS) a few conclusions can be summarized as follows; 1) all of the antireflection layers studied can effectively increase the performance of carbon nanotube-silicon solar cells by increasing the light absorbed by the silicon, resulting in increased J_{sc} and PCE, 2) the improvement is dependent on the thickness of the polymer layers (which determines the wavelength at which the minimum reflectance occurs), 3) antireflection layers composed of PS and PMMA which are spin coated onto devices provide better isolation from the atmosphere than PDMS applied by simple attachment, which has a limited protection effect. The best performing solar cell in this study, a Si-CNT-PS device with an optimal antireflection layer thickness, yielded a J_{sc} of 24.2 mA cm^{-2} and PCE of 7.8 % under AM1.5G illumination. This study confirms that the use of low-cost polymer antireflection layers is not only a viable strategy to obtain increased photocurrent from carbon nanotube-silicon solar cells without detriment to other important device characteristics, but has the additional benefit of significantly enhancing their long term stability.

Acknowledgements

This work is supported by the Australian Microscopy and Microanalysis Research Facility (AMMRF).

References

[1] Smalley, R.E., 2005. Future global energy prosperity: The terawatt challenge. MRS Bull. 30, 412-417.
[2] Chen, H. H. and Chen, S., 2014. The conceptual model for the strategic planning of energy sources. Energy Sources Part B 9, 248-255.
[3] Babu, V. J., Vempati, S., Sundarrajan, S., Sireesha, M., Ramakrishna, S., 2014. Effective nanostructured morphologies for efficient hybrid solar cells. Solar Energy 106, 1–22.
[4] Wu, Z. C., Chen, Z. H., Du, X., Logan, J. M., Sippel, J., Nikolou, M., Kamaras, K., Reynolds, J. R., Tanner, D. B., Hebard, A. F., Rinzler, A. G., 2004. Transparent, conductive carbon nanotube films. Science 305, 1273-1276.
[5] Ouyang, Y., Yoon, Y., Guo, J., 2007. On the current delivery limit of semiconducting carbon nanotubes. J. Comput.-Aided Mater. Des. 14, 73-78.
[6] Wijewardane, S., 2009. Potential applicability of CNT and CNT/composites to implement ASEC concept: A review article. Solar Energy 83, 1379–1389.
[7] Yan, J., Uddin, M. J., Dickens, T. J., Okoli, O.I., 2013. Carbon nanotubes (CNTs) enrich the solar cells. Solar Energy 96, 239–252.
[8] Tune, D. D., Flavel, B. S., Krupke, R., Shapter, J. G., 2012. Carbon nanotube-silicon solar cells. Adv. Energy Mater 2, 1043-1055.
[9] Jia, Y., Cao, A. Y., Bai, X., Li, Z., Zhang, L. H., Guo, N., Wei, J. Q., Wang, K. L., Zhu, H. W., Wu, D. H., Ajayan, P. M., 2011. Achieving high efficiency silicon-carbon nanotube heterojunction solar cells by acid doping. Nano Lett. 11, 1901-1905.
[10] Wei, J. Q., Jia, Y., Shu, Q. K., Gu, Z. Y., Wang, K. L., Zhuang, D. M., Zhang, G., Wang, Z. C., Luo, J. B., Cao, A. Y., Wu, D. H., 2007. Double-walled carbon nanotube solar cells. Nano Lett. 7, 2317–2321.

[11] Li, Z., Kunets, V. P., Saini, V., Xu, Y., Dervishi, E., Salamo, G. J., Biris, A. R., Biris, A. S., 2008. $SOCl_2$ enhanced photovoltaic conversion of single wall carbon nanotube/n-silicon heterojunctions. Appl. Phys. Lett. 93 243117.
[12]Mohammed, M., Li, Z., Cui, J., Chen, T.-P., 2014. Acid-doped multi-wall carbon nanotube/n-Si heterojunctions for enhanced light harvesting. Solar Energy 106, 171–176.
[13] Jia, Y., Li, P. X., Wei, J. Q., Cao, A. Y., Wang, K. L., Li, C. L., Zhuang, D. M., Zhu, H. W., Wu, D. H., 2010. Carbon nanotube films by filtration for nanotube-silicon heterojunction solar cells. Mater. Res. Bull. 45, 1401-1405.
[14] Wadhwa, P., Liu, B., McCarthy, M. A., Wu, Z. C., A.G. Rinzler, 2010. Electronic junction control in a nanotube-semiconductor Schottky junction solar cell. Nano Lett. 10, 5001-5005.
[15] Jia, Y., Li, P., Gui, X., Wei, J., Wang, K., Zhu, H., Wu, D., Zhang, L., Cao, A., Xu, Y., 2011. Encapsulated carbon nanotube-oxide-silicon solar cells with stable 10% efficiency. Appl. Phys. Lett. 98, 133115.
[16] Li, R., Di, J., Yong, Z., Sun, B., Li, Q., 2014. Polymethylmethacrylate coating on aligned carbon nanotube–silicon solar cells for performance improvement. J. Mater. Chem. 2, 4140.
[17] Shi, E. Z., Zhang, L. H., Li, Z., Li, P. X., Shang, Y. Y., Jia, Y., Wei, J.Q., Wang, K. L., Zhu, H.W., Wu, D, H., Zhang, S., Cao, A. Y., 2012. TiO_2-Coated Carbon Nanotube-Silicon Solar Cells with Efficiency of 15%. Sci. Rep. 2, 884.
[18] Wang, F., Kozawa, D., Miyauchi, Y., Hiraoka, K., Mouri, S., Ohno, Y. and Matsuda, K. 2015. Considerably improved photovoltaic performance of carbon nanotube-based solar cells using metal oxide layers. Nature Communications. 6, 6305.
[19] Ferry, D. K., Barker, J. R., 1980. On the physics and modeling of small semiconductor-devices. 3. transient-response in the finite collision-duration regime Solid-State Electron. 23, 545-549.
[20] Ryabenko, A. G., Dorofeeva, T. V., Zvereva, G. I., 2004. UV-VIS-NIR spectroscopy study of sensitivity of single-wall carbon nanotubes to chemical processing and Van-der-Waals SWNT/SWNT interaction. Verification of the SWNT content measurements by absorption spectroscopy. Carbon 42, 1523-1535.
[21] Dettlaff-Weglikowska, U., Shakalova, V., Graupner, R., Jhang, S. H., Kim, B. H., Lee, H. J., Ley, L., Park, Y. W., Berber, S., Tomanek, D., Roth, S., 2005. Effect of $SOCl_2$ treatment on electrical and mechanical properties of single-wall carbon nanotube networks. J. Am. Chem. Soc. 127, 5125-5131.
[22] Li, X., Yu, X. H., Han, Y. C., 2013. Polymer thin films for antireflection coatings. J. Mater. Chem. C 1, 2266-2285.
[23] Zhao, J., Green, M. A., 1991. Optimized antireflection coatings for high-efficiency silicon solar-cells. IEEE Trans. Electron Devices. 38, 1925-1934.
[24] Liu, R., Lee, S. T., Sun, B., 2014. 13.8% efficiency hybrid Si/organic heterojunction solar cells with MoO_3 film as antireflection and inversion induced layer. Adv Mater. 26, 6007-6012.
[25] Nakai, Y., Yoshimizu, H. Tsujita, Y. 2006. Enhancement of Gas Permeability in HPC, CTA and PMMA under Microwave Irradiation. Polymer Journal. 38, 376-380.
[26] Horák, Z., Kolařík, J., Šípek, M., Hynek, V., Večerka, F., 1998. Gas Permeability and Mechanical Properties of Polystyrene–Polypropylene Blends. Journal of Applied Polymer Science. 69, 2615-2623.
[27] Merkel, T. C., Bondar, V. I., Nagai, K., Freeman, B. D., Pinnau, I. 2000. Gas Sorption, Diffusion, and Permeation in Poly(dimethylsiloxane). Journal of Polymer Science Part B: Polymer Physics. 38, 415-434.
[28] Jia, Y., Cao, A. Y., Kang, F. Y., Li, P. X., Gui, X. C., Zhang, L. H., Shi, E. Z., Wei, J. Q., Wang, K. L., Zhu, H. W., Wu, D. H., 2012. Strong and reversible modulation of carbon nanotube-silicon heterojunction solar cells by an interfacial oxide layer. Phys. Chem. Chem. Phys. 14, 8391-8396.
[29] Jung, Y., Li, X., Rajan, N. K., Taylor, A. D., Reed, M.A. 2013 Record High Efficiency Single-Waaled Carbon Nanotube/Silicon p-n Juction Solar Cells, Nano Letters 13, 95-99.

Supplementary information

Table S1: The variation of properties of Si-CNT device after each post treatment. Resistances were calculated from light curves

	As prepared	**1st HF**	**$SOCl_2$**	**2nd HF**
Ideality	4.9	2.0	4.5	1.5
J_{sat} (mA cm^{-2}):	4.72×10^{-3}	4.65×10^{-4}	2.04×10^{-3}	8.20×10^{-5}
R_{shunt}(Ohms)	2.67×10^{3}	5.73×10^{2}	3.05×10^{2}	1.66×10^{5}
R_{series}(Ohms)	8.08×10^{4}	5.27×10^{2}	3.98×10^{3}	9.72×10^{1}

Table S2: Full error analysis of the influence of different antireflection layers on the performance of Si-CNT devices.

PDMS Cells

	Control without PDMS					With PDMS				
	Cell 1	Cell 2	Cell 3	Average	Std. Dev.	Cell 1	Cell 2	Cell 3	Average	Std. Dev.
J_{sc} (mA cm^{-2})	18.9	17.9	18.5	18.4	0.50	19.9	18.8	19.8	19.5	0.61
V_{oc} (V)	0.52	0.49	0.5	0.50	0.015	0.52	0.48	0.49	0.50	0.02
FF	0.68	0.63	0.61	0.64	0.03	0.68	0.63	0.61	0.64	0.04
Eff (%)	6.63	5.52	5.64	5.93	0.61	6.93	5.68	5.91	6.17	0.67
R_{shunt} (Ω) (x 10^{-4})	2.56	6.77	5.35	4.89	2.14	9.44	9.89	8.79	9.37	0.55
R_{series} (Ω)	67.5	89.7	78.6	78.6	11.1	61.5	83.3	86.8	77.2	13.7

PMMA Cells

	Control without PMMA					With PMMA				
	Cell 1	Cell 2	Cell 3	Average	Std. Dev.	Cell 1	Cell 2	Cell 3	Average	Std. Dev.
J_{sc} (mA cm^{-2})	17.9	18.5	17.3	17.9	0.6	20.2	21.2	19.8	20.4	0.72
V_{oc} (V)	0.52	0.5	0.5	0.51	0.01	0.51	0.5	0.49	0.5	0.01
FF	0.69	0.65	0.65	0.66	0.02	0.67	0.62	0.63	0.64	0.03
Eff (%)	6.31	6.01	5.62	5.98	0.35	6.95	6.57	6.11	6.54	0.42
R_{shunt} (Ω) (x 10^{-4})	1.71	1.88	9.86	4.48	4.65	0.77	0.85	0.97	0.86	0.10
R_{series} (Ω)	69.4	72.5	88.7	76.8	10.4	61.1	68.7	80.5	70.1	9.8

PS Cells

	Control without PS					With PS				
	Cell 1	Cell 2	Cell 3	Aver.	Std. Dev.	Cell 1	Cell 2	Cell 3	Aver.	Std. Dev.
J_{sc} (mA cm^{-2})	19.6	17.7	17.9	18.4	1.0	24.1	22.1	21.7	22.6	1.28
V_{oc} (V)	0.53	0.52	0.51	0.52	0.01	0.51	0.5	0.5	0.50	0.01
FF	0.69	0.67	0.63	0.66	0.031	0.63	0.63	0.6	0.62	0.017
Eff (%)	7.02	6.17	5.75	6.31	0.65	7.84	6.96	6.51	7.10	0.68
R_{shunt} (Ω) (x 10^{-4})	12.8	1.30	8.45	7.52	5.81	0.49	0.58	9.77	3.61	5.33
R_{series} (Ω)	66.4	69.8	78.9	71.7	6.47	60.0	63.6	68.7	64.1	4.37

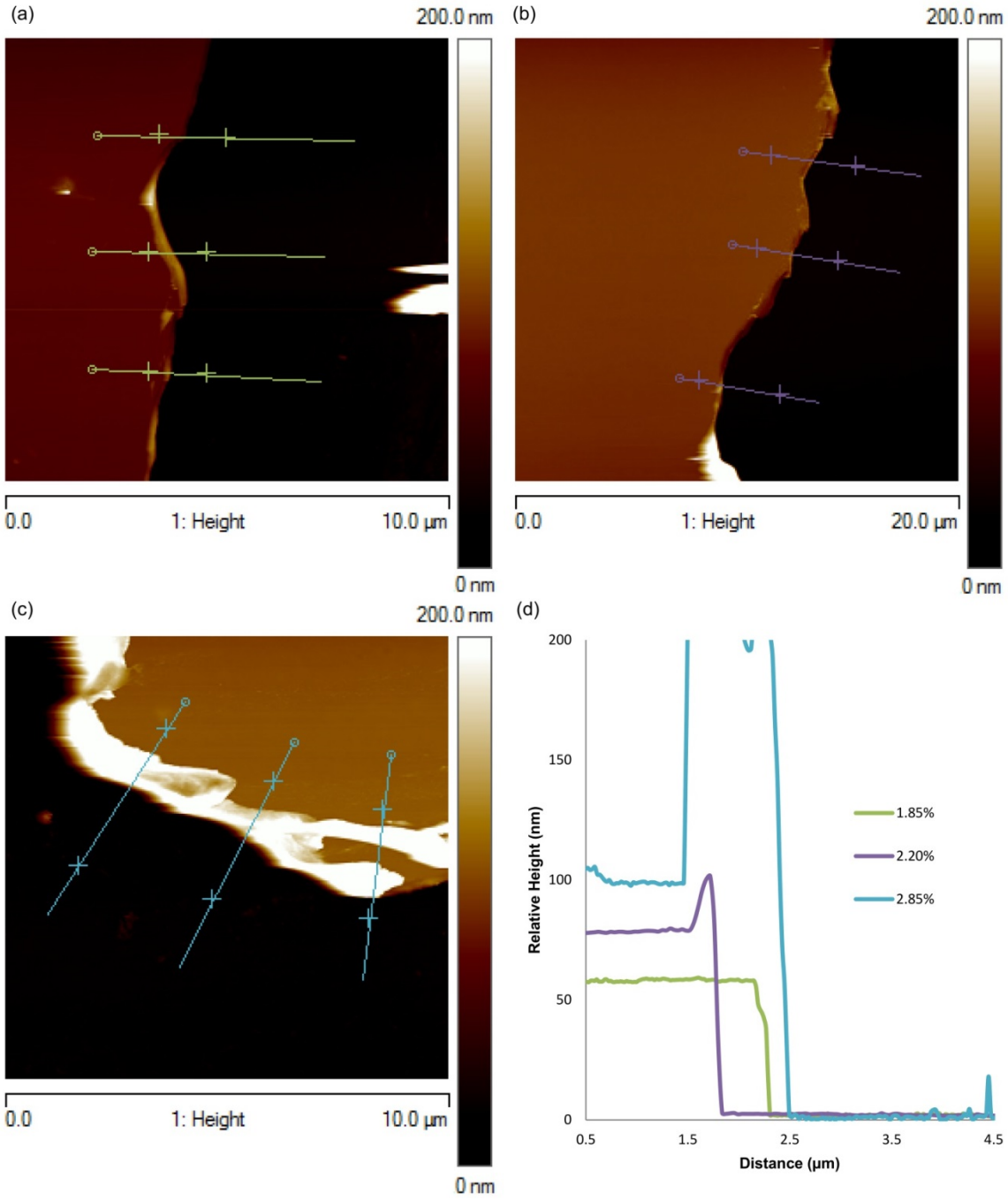

Figure S1: AFM height images of PS films spin coated onto Si surfaces from different concentration solutions of (a) 1.85 wt%, (b) 2.2 wt% and (c) 2.85 wt% in toluene (lines and cross markers are used to indicate where the thickness measurements were made) and (d) relative height curves across the boundary between Si and PS surfaces of different thickness.

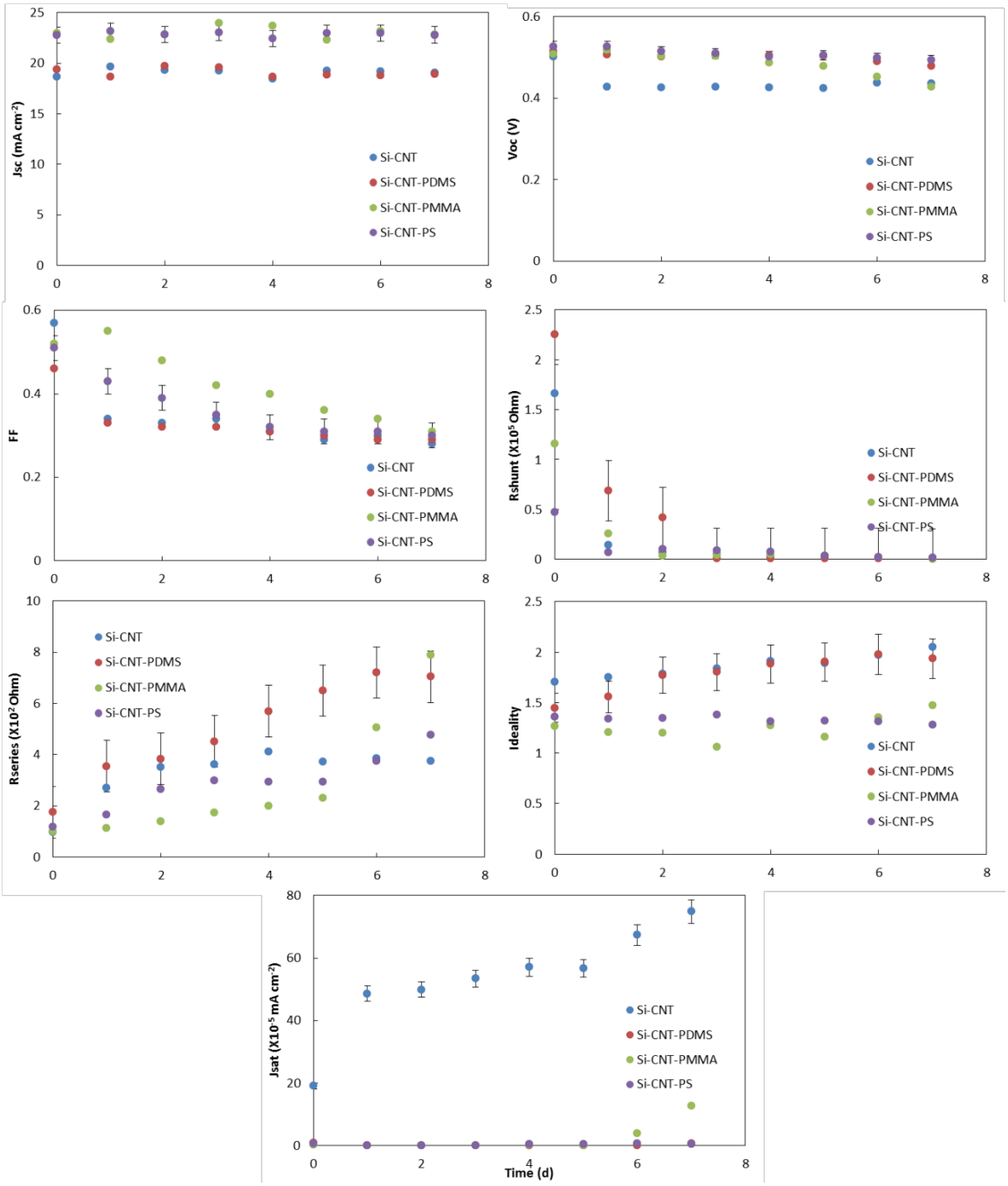

Figure S2: Degradation comparison of Si-CNT, Si-CNT-PDMS, Si-CNT-PMMA and Si-CNT-PS over 7 days: (a) J_{sc}, (b) V_{oc}, (c) FF (d) R_{shunt} (e) R_{series} (f) ideality and (g) J_{sat}. Error bars shown are one standard deviation. The error bars for the other data are very similar but not shown for clarity.